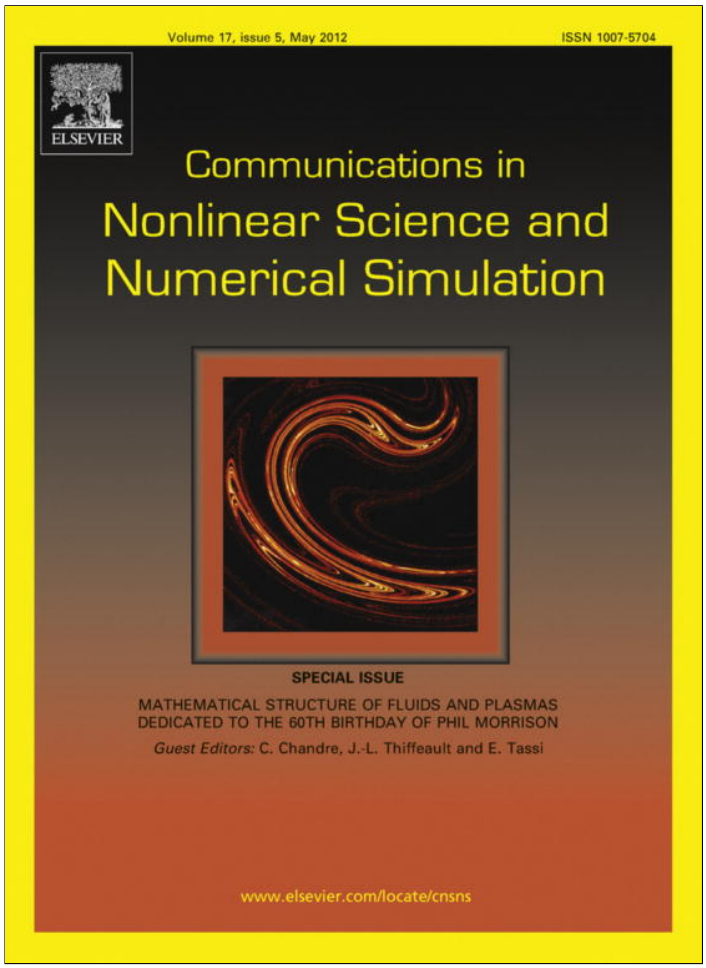

Commun Nonlinear Sci Numer Simulat 17 (2012) 1989–1997

Contents lists available at ScienceDirect

Commun Nonlinear Sci Numer Simulat

journal homepage: www.elsevier.com/locate/cnsns

BGK states from the bump-on-tail instability

N.J. Balmforth

Departments of Mathematics and Earth & Ocean Science, University of British Columbia, Vancouver, Canada

ARTICLE INFO

Article history:
Available online 23 July 2011

Keywords:
Plasma instability
Vlasov–Poisson equation
BGK modes

ABSTRACT

Numerical computations are presented of the BGK-like states that emerge beyond the saturation of the bump-on-tail instability in the Vlasov–Poisson system. The stability of these states towards subharmonic perturbations is explored in order to gauge whether the primary bump-on-tail instability always suffers a secondary instability that precipitates wave mergers and coarsening of the BGK pattern. Because the onset of the bump-on-tail instability occurs at finite wavenumber, and the spatially homogeneous state is not itself unstable to spatial subharmonics, it is demonstrated that mergers and coarsening do not always occur, and the dynamics displays a richer spatio-temporal complexity.

1. Introduction

BGK modes are steadily propagating nonlinear solutions to the Vlasov–Poisson and related systems [5]. These modes can be excited by introducing a sufficiently strong wave-like perturbation to a stable, spatially homogenous equilibrium, such that nonlinearity arrests Landau damping (*e.g.* [21,16,7]). Alternatively, BGK-like modes can emerge due to the nonlinear saturation of the linear instabilities of an unstable homogeneous equilibria (*e.g.* [1,2,10,13]).

It is commonly viewed that periodic BGK modes are prone to secondary instabilities whenever the spatial domain contains more than one wavelength. The secondary instability precipitates a coarsening event wherein waves interact and merge to increase the wavelength until only a single wave survives in the domain [10]. Mathematical arguments to back up this vision have been advanced by Goldman [11], Schwarzmeier et al. [24], Guo and Strauss [12] and Lin [14,15], who present various types of stability analyses of BGK modes. A number of thermodynamic arguments in support of coalescence have also been advanced [19,9,23].

Fig. 1 illustrates the secondary instability and merger dynamics for the classical bump-on-tail instability: the simulation takes place in a periodic spatial domain, and is arranged so that the second (spatial) Fourier mode is excited at low amplitude at the beginning of the computation; that mode then amplifies exponentially until it twists up the background distribution into a BGK-like state propagating in the vicinity of the bump. The state is unsteady due to "trapping" oscillations (*e.g.* [25]), but for a while the mean electrostatic potential saturates at an average level. However, the fundamental Fourier mode, which was excited to a much lower amplitude at the initialization of the computation grows all the while. Eventually this mode reaches sufficient strength to disturb the cat's-eye-like pattern generated by the original instability, triggering a merger event and the formation of a longer-scale, unsteady BGK-like state.

The purpose of the present article is to present detailed numerical computations of the nonlinear dynamics of the classical bump-on-tail instability, and thereby demonstrate that BGK-mode phenomenology is not as clear cut as the previous articles suggest. In particular, we show that coarsening mergers do not always result from BGK-mode secondary instabilities in the bump-on-tail problem. Moreover, BGK modes with multiple wavelengths can even be stable (in periodic domains of suitable length).

E-mail address: njb@math.ubc.ca

1007-5704/$ - see front matter © 2011 Elsevier B.V. All rights reserved.
doi:10.1016/j.cnsns.2011.07.022

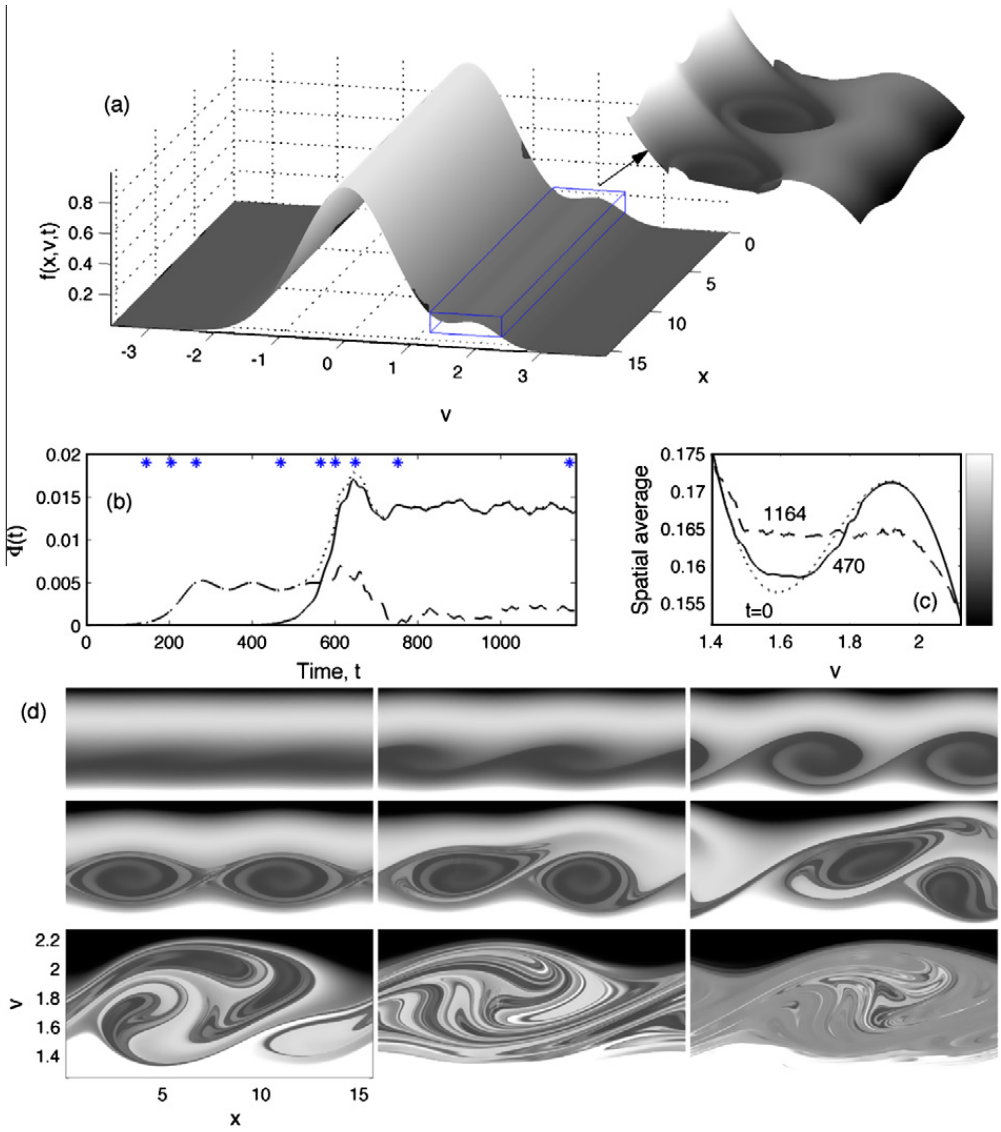

Fig. 1. Vlasov simulation for the equilibrium in (8) with $a = 0.15$ and $L = 5\pi$. The potential $\varphi(x,t)$ is forced initially by adding $te^{-10t^2}(10^{-3}\cos 4\pi x/L + 10^{-6}\cos 2\pi x/L)$ to (4). (a) shows the initial distribution, plus a magnification of the bump region at $t = 260$. Panel (b) shows a time series of the first two Fourier mode amplitudes of the potential, $|\Phi_1(t)|$ (solid) and $|\Phi_2(t)|$ (dashed), together with the total amplitude, $\Phi(t)$ (dotted); see Eqs. (4) and (5). Panel (c) displays the spatial average of the distribution function, $f(x,v,t)$, in the vicinity of the bump at the times indicated. The stars in (b) indicate the times at which nine snapshots of $f(x,v,t)$ are shown in (d) as densities on the (x,v)-plane (again focussing on the bump). The shading scheme is indicated by (c) (the dynamics amounts to a rearrangement of $f(x,v,0)$).

A key detail that distinguishes the bump-on-tail problem from other BGK-mode producing instabilities, such as the two-stream instability, is that the primary instability sets in with a finite wavenumber. In dissipative systems, this sets the stage for spatio-temporal complexity (the weakly nonlinear description is the complex Ginzburg–Landau equation, a popular model for studying chaotic dynamics in spatially extended systems; *e.g.* [18]). For the plasma problem, it signifies that close enough to onset, the spatially homogeneous state is stable towards perturbations with smaller wavenumbers (the subharmonics of the primary instability). Not only does this negate the existing theories that establish subharmonic instability of the primary BGK patterns that may form [12,17], but it also indicates that there may be no suitable BGK modes that can act as end states for a coarsening event. Indeed, instead of coarsening, the numerical computations reported below reveal a much richer time-dependent dynamics. The example shown in Fig. 1 does not display this dynamics, as it lies in a parameter regime much further from onset, where the subharmonic of the primary instability (the fundamental Fourier mode) is already strongly unstable.

2. Mathematical formulation

2.1. The dimensionless Vlasov–Poisson system

The dimensionless Vlasov-Poisson system for the distribution function, $f(x,v,t)$, and electrostatic potential, $\varphi(x,t)$, can be written in the form,

$$f_t + vf_x + \varphi_x f_v = 0, \tag{1}$$

$$\varphi_{xx} = \int_{-\infty}^{\infty} f(x,v,t)\,\mathrm{d}v - \langle f\rangle, \tag{2}$$

where

$$\langle \ldots \rangle \equiv \int_{-\infty}^{\infty}\int_0^L (\ldots)\frac{\mathrm{d}x}{L}\,\mathrm{d}v, \tag{3}$$

L is the length of the (periodic) spatial domain, and the (x,v,t) subscripts denote partial derivatives. To arrive at this dimensionless form of the Vlasov equation, we scale time by the inverse plasma frequency ω_p^{-1}, space by the Debye length λ_D, and speed by $\omega_p\lambda_D$. The potential can also be represented in terms of its spatial Fourier series,

$$\varphi = \sum_{n=-\infty}^{\infty} \Phi_n \mathrm{e}^{2\pi \mathrm{i} n x/L}, \quad \Phi_n(t) = \frac{1}{L}\int_0^L \varphi(x,t)\mathrm{e}^{-\mathrm{i}nx}\,\mathrm{d}x, \tag{4}$$

and mean amplitude,

$$\Phi(t) = \left[\sum_{n=0}^{\infty} |\Phi_n|^2\right]^{1/2}. \tag{5}$$

2.2. Linear theory

The spatially homogeneous solutions to (1) are characterized by a profile, $f(x,v,t) = F(v)$. We explore normal-mode perturbations about such equilibria by setting

$$f = F(v) + \hat{f}(v)\mathrm{e}^{\mathrm{i}k(x-ct)}, \tag{6}$$

where k is the wavenumber and c is the wavespeed. After introducing this decomposition into (1) and (2) and then linearizing in the amplitude, $\hat{f}(v)$, one arrives at the familiar dispersion relation,

$$D(c) = k^2 - \int_{\infty}^{\infty} \frac{F'(v)}{v-c}\,\mathrm{d}v. \tag{7}$$

By way of example, we consider the family of equilibria given by

$$F(v) = \mathrm{e}^{-v^2} + a\mathrm{e}^{-(v-v_0)^2/\sigma^2}, \tag{8}$$

where a, v_0 and σ are parameters. The distribution in (8) takes the form of a main Maxwellian centred at zero speed together with an additional Gaussian bump at $v = v_0$ of strength a and half-width, σ. In practice, we adopt $v_0 = 2$ and $\sigma = 1/2$, then vary a in order to trigger a linear instability. Numerical results displaying the unstable region of the (k,a)-plane are shown in Fig. 2.

2.3. Numerical scheme

We solve Eqs. (1) and (2) numerically using an operator-splitting scheme [6]. This scheme divides the time integration into two advection steps. Advection in x is performed using the fast Fourier transform on a uniform grid of N points, and

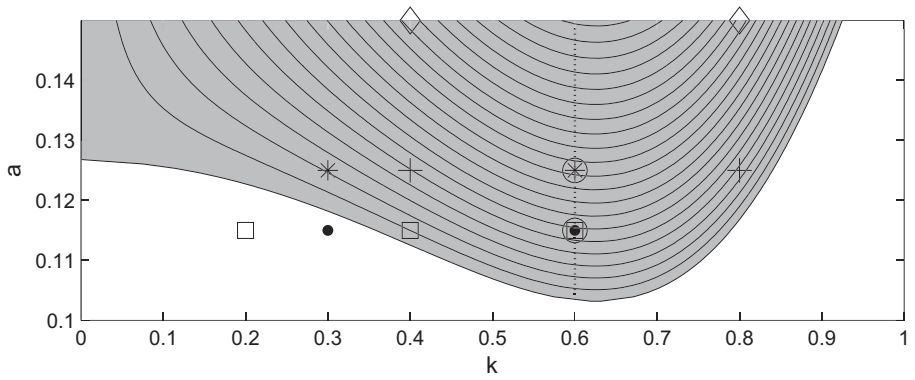

Fig. 2. Unstable region of the (k,a)-plane (shaded). The curves show contours of constant growth rate, spaced by 0.002 and starting at zero. Also indicated are the important modes in the simulations of Fig. 1 (diamonds), Fig. 5 (dots), Fig. 6 (squares), Fig. 7 (crosses), and Fig. 10 (stars). The circles and vertical dotted line refer to computations shown in Fig. 3. Here, as throughout, the equilibrium is given by (8) with $v_0 = 2$ and $\sigma = 1/2$.

advection in v using spline interpolation on a grid of M points distributed over the truncated interval, $[-v_{max}, v_{max}]$. The grid in v is non-uniform, with a finer grid spacing placed over the region of the bump in order to resolve the dynamics there. Typically, we take $N = 512$ and $M = 2500$, with the grid in v arranged so that there are more than 600 intervals over the bump region ($1.55 < v < 1.95$) and $v_{max} > 4$. The time step was 0.01 or less.

To initialize the computations, we use the equilibrium in (8), and then kick the system into action by adding a suitable forcing term to the potential in (4), as summarized in the captions to the figures. We select this device to initiate the dynamics because it mimics an electrostatic forcing of a physical system and because it generates a "dynamically accessible" rearrangement of the equilibrium [20]. However, we could also have begun by directly perturbing the distribution function; the main results are unlikely to be any different given that the main effect of the initial perturbation is to excite at low amplitude a particular normal mode.

3. Results

3.1. Basic BGK states

To begin, we first summarize the characteristics of the basic nonlinear states that emerge from the saturation of the bump-on-tail instability in spatial domains containing a single wavelength. Fig. 3 shows a simulation with $a = 0.115$ in a domain of length $10\pi/3$, for which there is a single unstable mode with $k = 0.6$. Initially, the mode amplifies exponentially with the growth rate predicted by linear theory, but then saturates by twisting up the distribution over the region of the bump into a cat's eye pattern. This generates a nonlinear state similar to a BGK mode. However, aperiodic trapping oscillations also arise, and it is unclear for how long they persist [25]. The saturated nonlinear solutions are, therefore, not exactly equivalent to steady BGK modes, but in view of their similarity to those waves, we call them "BGK states".

Fig. 3 also plots the maximum amplitude, Φ_m, against the distance to the stability boundary ($a - a_*$, with $a_* \approx 0.1034$), for a suite of computations with $L = 10\pi/3$; this saturation measure follows the trapping scaling of O'Neil et al. [22] (see also [4]). The scaling is relatively weak and signifies that the re-arrangements of the equilibrium distribution in the vicinity of the bump cannot fully smooth out that feature. This is illustrated by the final spatial average of $f(x, v, t)$ for $a = 0.115$ shown in Fig. 3(d).

Steady BGK waves are characterized by a functional relation, $f(x, v, t) = \mathcal{F}(\mathcal{E})$, between particle energy in the waveframe, $\mathcal{E} = \frac{1}{2}(v - c)^2 - \varphi$, and distribution function, where c is the wavespeed. In general, $\mathcal{F}(\mathcal{E})$ is a multi-valued function with different pieces corresponding to the phase space above, below or inside the cat's eye patterns. Fig. 4 plots the relationship between $\mathcal{E}$ and f for the final solution of Fig. 3. Everywhere except in the vicinity of the bump, the $f - \mathcal{E}$ relation is equivalent to that of the initial condition (with $\varphi = 0$); but over that region, the overturning within the cat's eye mixes up the $(f, \mathcal{E})$−values to generate a broad cloud of points. In a coarse-grained sense, it is possible that the system eventually relaxes to a true, steady BGK mode characterized by a single-valued $f - \mathcal{E}$ relation within the cat's eye. However, the state in Fig. 4 has yet to mix up in such a fashion and remains agitated by trapping oscillations. There is some suggestion from Fig. 4 that, if relaxation

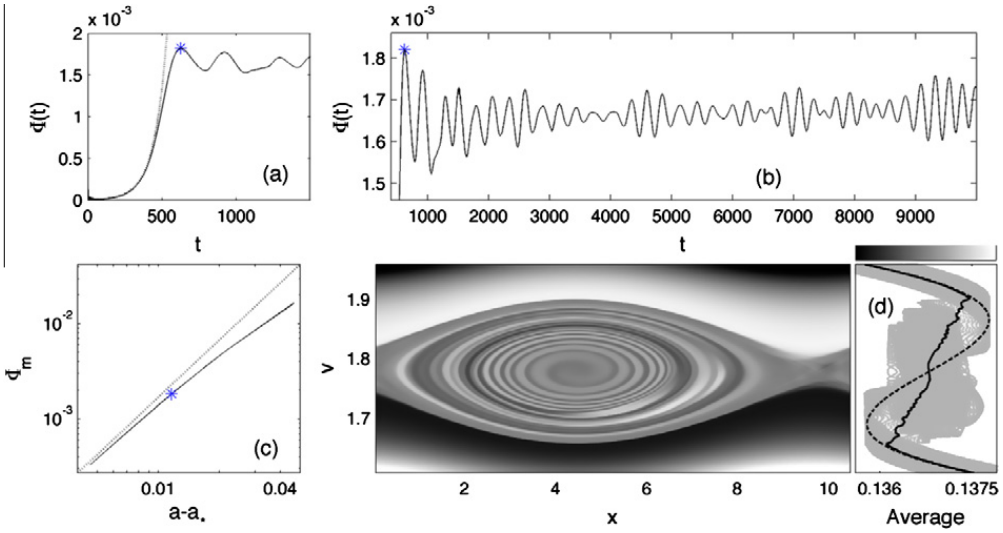

Fig. 3. Simulation for $a = 0.115$ in a domain of length $L = 10\pi/3$, initiated by adding $10^{-3}te^{-10t^2}$ to $\Phi_1(t)$. Panels (a) and (b) show $\Phi(t)$; the dotted line in (a) shows the exponential growth expected from linear theory. In (c) the value of the first maximum, Φ_m (indicated by stars in (a) and (b)), is plotted against the distance to the stability boundary, $a - a_*$ (where $a_* \approx 0.1034$ is the marginally stable state) for a suite of computations with varying a, along with the trend of trapping scaling of [22], $\Phi_m \propto (a - a_*)^2$. A snapshot of the final ($t = 10^4$) cat's eye pattern in $f(x, v, t)$ is shown as a density on the (x, v)-plane in (d). To interpret the shading scheme, the plot to the right shows the spatial average (solid), equilibrium profile (dashed) and all the values of $f(x, v, t)$ on the computational grid (light gray dots).

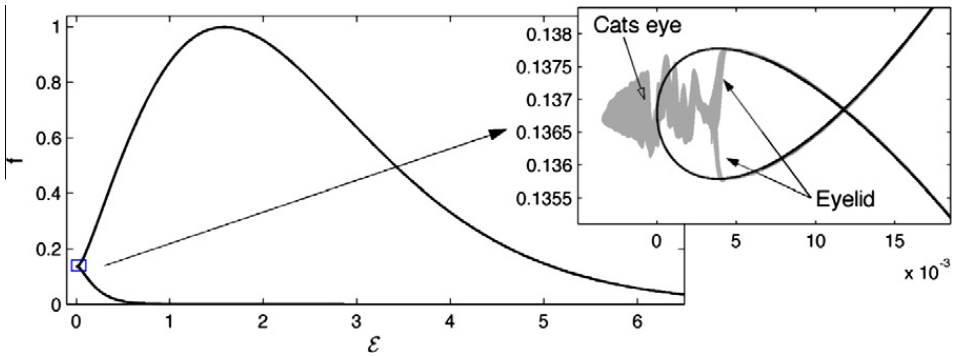

Fig. 4. Plots of energy, $\mathcal{E} = \frac{1}{2}(v-c)^2 - \varphi$, against $f(x,v,t)$ at all points on the computational grid (light gray dots) for the solution also shown in Fig. 3; $c \approx 1.778$. The solid line shows the initial condition.

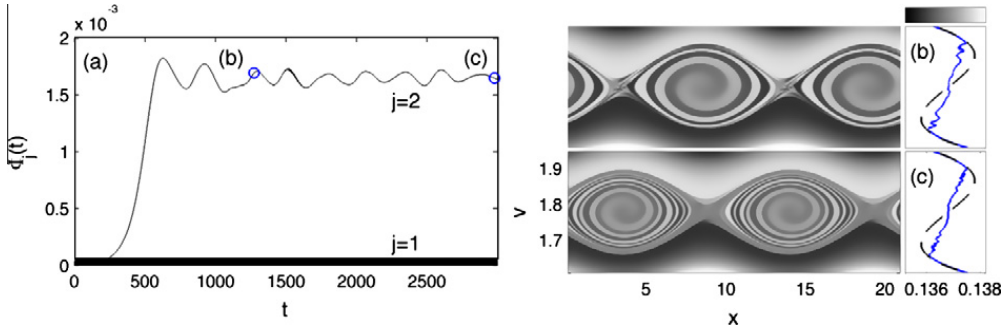

Fig. 5. Simulation with $a = 0.115$ in a domain of length $L = 20\pi/3$, initiated by adding $10^{-3}te^{-10t^2}$ to $\Phi_1(t)$ and $\Phi_2(t)$. Panel (a) shows $|\Phi_j(t)|$, for $j = 1$ and 2. The circles mark the times at which snapshots of the cat's-eye patterns in $f(x,v,t)$ are shown as densities on the (x,v)-plane in (b)–(c); the spatial averages (solid) and initial profiles (dashed) on the right indicate the shading scheme.

does occur, the cat's eye $f - \mathcal{E}$ relation may become flat, with sharp boundary layers along the eyelids separating that constant from the double-valued $f - \mathcal{E}$ relation characterizing the regions outside the cat's eye. Note that the $f - \mathcal{E}$ relation may have an infinite derivative along the cat's eyelid, as implied by coarse-grained averages [3] of O'Neil's analytical solution of nonlinear Landau damping [21].

Despite this suggestion that the cat's eye distribution may become flat, there are distinct undulations in the $f - \mathcal{E}$ relation near the eyelids. These correspond to the ring-like features discernible in the spatial structure of $f(x,v,t)$ in Fig. 3(d), and result from coherent secondary structures, or "quasi-particles" [25], which circulate around the cat's eyes (two such features are visible to the lower right of the cat's eye in Fig. 3(d)). The quasi-particles themselves are intimately connected to the trapping oscillations.

Note that the lack of symmetry between the regions above and below the cat's eye renders the linear stability analysis of the BGK mode more complicated than assumed by Lin [14]. He presents a formal analysis suggesting that BGK modes with more than one wavelength in the spatial domain are unstable (and establishes a more rigorous foundation for some incomplete arguments made earlier by Ghizzo et al. [10]). However, the arguments rely on the self-adjointness of a operator which only takes that form provided the $f - \mathcal{E}$ relation is symmetrical above and below the cat's eye. The BGK modes that emerge if the trapping oscillations subside in Fig. 4 do not have this symmetry, and the operator arising in the corresponding stability theory is not self-adjoint. Thus Lin's analysis is not relevant to the bump-on-tail problem. Indeed, his results cannot apply in this situation since they imply that BGK modes of wavenumber k are always unstable to subharmonics with wavenumber $k/2$. But these BGK modes share the stability properties of the homogeneous equilibrium state as they approach the stability boundary [12], and linear stability theory demonstrates that such subharmonic instabilities do not always occur (see Fig. 2).

3.2. Searching for secondary instability

We now consider whether the BGK states described above suffer secondary instability. We commence with a computation for $a = 0.115$ and a domain of size $20\pi/3$ (so the wavenumbers are $0.3j$, $j = 1,2,\ldots$). After weakly forcing the potential with the first two Fourier modes, the system evolves as shown in Fig. 5. At these parameter settings, the fundamental is stable, but the first overtone is linearly unstable (Fig. 2). The overtone does indeed amplify as expected, and again saturates by twisting up the distribution near the bump into a pair of cat's eyes. Over the duration of this computation, the fundamental mode oscillates at low amplitude, but does not grow (such persistent ringing is not surprising: the corresponding spatially homogeneous equilibrium has very weakly decaying "quasi-modes" [4] with $k = 0.3$). Thus, there is little sign of a secondary instability for this "double" BGK state.

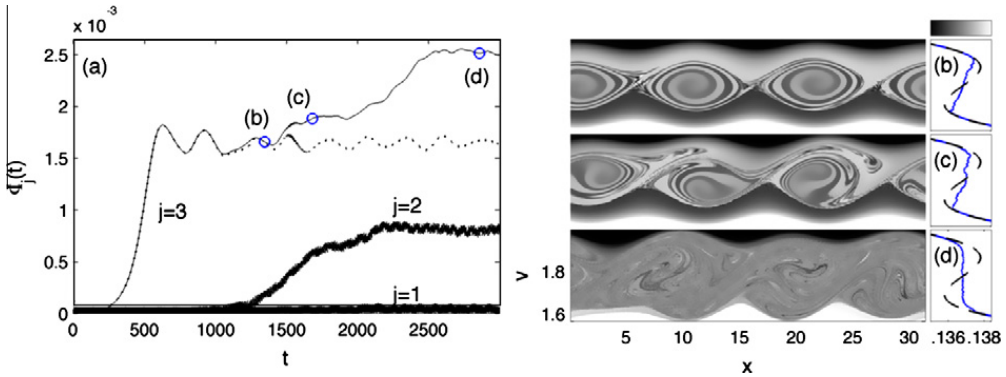

Fig. 6. Simulation with $a = 0.115$ in a domain of length $L = 10\pi$, initiated by adding $10^{-3}te^{-10t^2}$ to $\Phi_j(t)$, $j = 1$ to 3, with $|\Phi_j(t)|$ shown in (a); the dotted line shows $|\Phi_2|$ for the computation presented in Fig. 5. The circles mark the times of the snapshots shown in (b)–(d); the spatial average and initial profile on the right indicate the shading scheme.

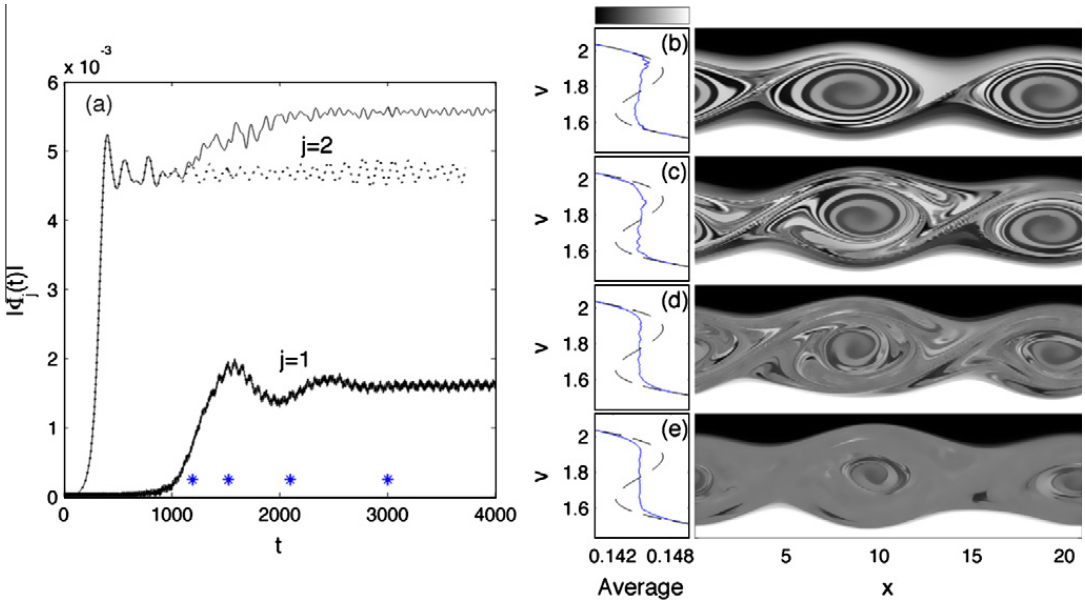

Fig. 7. Simulation with $a = 0.125$ in a domain of length $L = 20\pi/3$, initiated by adding the forcing, $10^{-3}te^{-10t^2}$, to the first two Fourier modes of the potential. Solid lines in (a) indicate $|\Phi_j|$ with $j = 1$ and 2; the dot-dashed line shows the computation of Fig. 8 in which the $j = 1$ mode is much more weakly forced. Stars indicate the times of the snapshots of (b)–(e); the spatial average and initial profile to the left indicate the shading scheme.

By contrast, when we widen the domain to $L = 10\pi$, and initialize by kicking the first three Fourier modes, we do observe a clear secondary instability; see Fig. 6. In this example, the $k = 0.6$ mode (the second overtone) is still the strongest instability and the fundamental mode ($k = 0.2$) is again linearly stable. However, the $k = 0.4$ mode (the first overtone) is also unstable, with a relatively small growth rate ($kc_i = 2 \times 10^{-3}$, versus 0.0116 for $k = 0.6$). At the beginning of the computation, the $k = 0.6$ mode dominates the linear growth and a triple cat's eye pattern forms over the bump region. This BGK state does not persist indefinitely, but becomes disrupted by the growth of a subharmonic corresponding to the $k = 0.4$ mode; see Fig. 6.

Similarly, when we increase the bump parameter, we also observe the double BGK state to suffer subharmonic secondary instability; see Fig. 7 for $a = 0.125$. Notably, as indicated by Fig. 2, for this parameter setting, the $k = 0.3$ fundamental mode of the homogeneous state is now unstable. Thus, the secondary instabilities of the finite-amplitude BGK states appear to be closely connected to the instabilities of the homogeneous state, as already concluded by Guo and Strauss [12] (see also [17]) for BGK states of arbitrarily small amplitude.

Further details of a secondary instability are shown in Fig. 8. In this simulation, at $a = 0.125$ and $L = 20\pi/3$, the computation is initialized with a low-amplitude $k = 0.6$ disturbance, but no subharmonic; the resulting instability is then allowed to grow and saturate for a time. At $t = 1500$, the subharmonic is then kicked into action by suitably forcing the Fourier amplitude, Φ_1, and thereafter is observed to grow exponentially (with a rate close to 0.008, twice the growth rate of the $k = 0.3$ mode of the spatially homogeneous equilibrium, $kc_i \approx 0.004$). By formulating the combination, $f(x, v, t) - f(x - L/2, v, t)$, we construct a corresponding "unstable mode". As shown in Fig. 8, the structure of the mode is relatively complicated, with a tightly wound spiral component within the cat's eyes together with a wave-like perturbation riding along the outer eyelids.

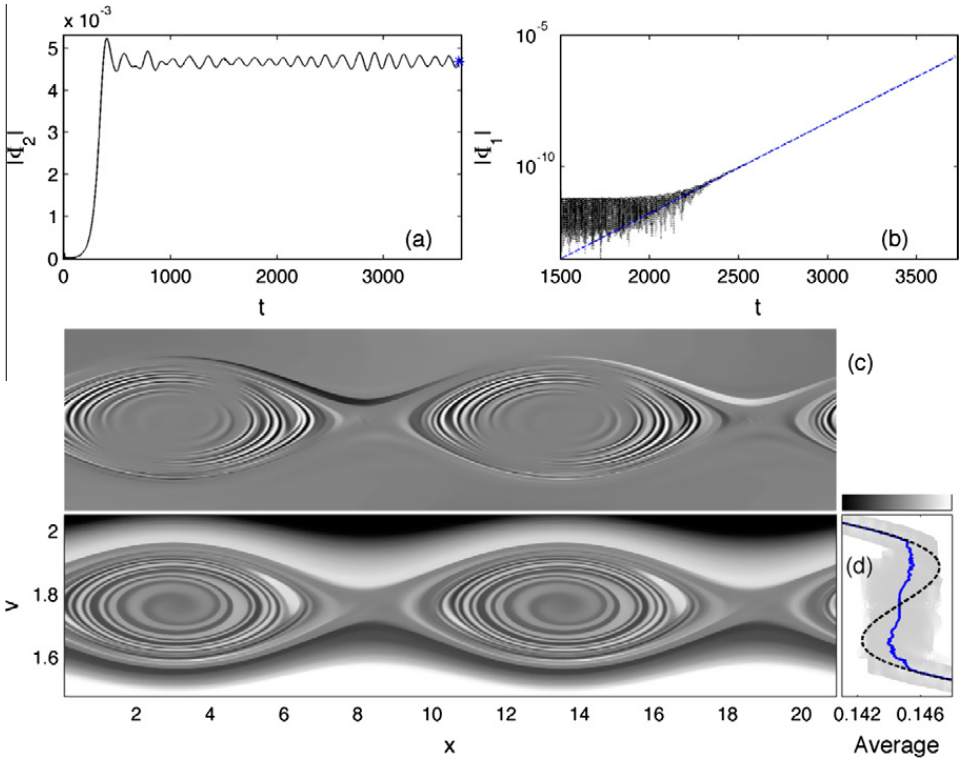

Fig. 8. Simulation disturbing a saturated BGK state with $k = 0.6$ and $a = 0.125$ in a domain of length $20\pi/3$. At $t = 1500$, Φ_1 (previously zero) is forced by $10^{-10}(t-1500)e^{-10(t-1500)^2}$. Panels (a) and (b) show the times series of $|\Phi_j(t)|$ for $j = 2$ and 1, respectively. The dashed line in (b) indicates exponential growth with a rate of 0.008; the star in (a) shows the time of the snapshot plotted in (c) and (d). Panel (c) shows the structure of the "unstable mode", as given by $f(x,v,t) - f(x - L/2, v, t)$; (d) shows the corresponding cat's eye pattern with the shading scheme indicated by the plots of the spatial average, the initial profile (dashed), and the values of $f(x,v,t)$ at the grid points (light gray dots). We omit the scale in (c) as the mode amplitude should be arbitrary.

Note that, although the computation shown in Fig. 5 reveals no subharmonic instability one cannot rule the possibility of instability since the trapping oscillations of the cat's eye patterns and the persistent ringing of the $j = 1$ mode obscure the dynamics. Moreover, the computations are less reliable over the longer times due to the filamentation of $f(x,v,t)$ and the smoothing resulting from finite resolution. In fact, when the computation is continued for much longer than is shown in Fig. 5 there is some evidence for a growing mode like that shown in Fig. 8, but with a much lower growth rate (order 10^{-3} or less). On the other hand, when a is reduced to 0.1125, even that evidence disappears and the double BGK states seem to be genuinely stable for as long as the computation is run. Thus, we conclude that subharmonic instabilities probably appear a finite distance beyond the stability boundary (for a just below 0.115 with $L = 20\pi/3$), and there is window of parameter space over which BGK states with muliple wavelengths in the domain can be stable.

3.3. To merge or not to merge

An important detail of all the computations of Section 3.2 is that there are no merging events: secondary instabilities grow and force recognizable distortions of the BGK patterns, but the dominant wavenumber remains largely unchanged. For example, in Fig. 7, there is little suggestion that a merger will occur despite the continuation of the simulation to a time well beyond the growth of the subharmonic. Indeed, the amplitude of the subharmonic mode has clearly saturated and the system appears to be converging to some (unsteady) asymptotic state. Note how the agitation of the primary BGK state prompts it to expand and more effectively mix, flattening out any residual bump in the average distribution.

To gauge whether mergers are ever likely in the parameter regime studied in Section 3.2, we performed further computations in which we first prepared a BGK state with a single wavelength by running a computation with $L = 10\pi/3$ out to $t = 1500$. The domain was then doubled, and the distribution, $f(x,v,t)$, perturbed by adding $\alpha e^{-4(v-2)^2}\cos(2\pi x/L)$, where the strength parameter, α, was varied. Three such computations for $a = 0.115$ are shown in Fig. 9, with $\alpha = 10^{-6}$, 10^{-4} and 10^{-3}. In the first case, the subharmonic mode does not amplify over the duration of the computation. The stronger perturbations, however, generate noticeable disturbances in the BGK patterns, and there is some growth of the subharmonic beyond the initial perturbation (see the dots in Fig. 9(a) for $\alpha = 10^{-4}$; the persistent ringing of this mode obscures the picture for $\alpha = 10^{-3}$ and so we have plotted the running average, $(t-1500)^{-1}\int_{1500}^{t}|\Phi_1|\,dt$, instead). We interpret this growth to be due to an expansion of the region in which the equilibrium distribution is twisted up, which draws in more of the destabilizing background gradients and suppresses more of the bump. This growth is difficult to rationalize as a secondary instability of the primary BGK state, and appears to be mostly due to the finite amplitude of the disturbance. Indeed, the two cases, $\alpha = 10^{-4}$ and 10^{-3}, converge to quite different end-states.

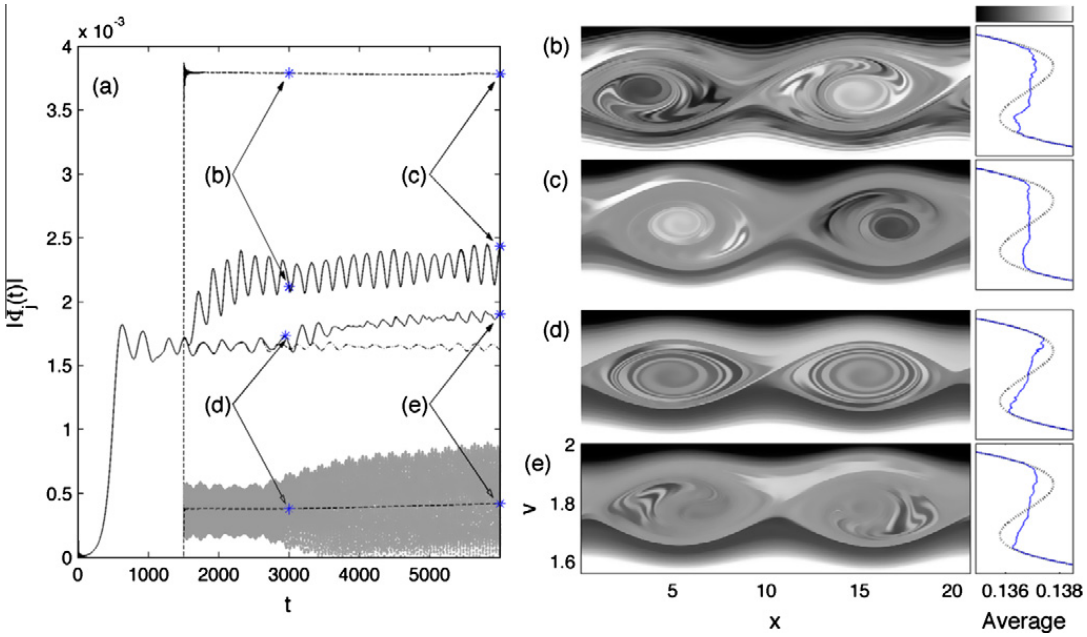

Fig. 9. Simulations disturbing saturated BGK states with $k = 0.6$ and $a = 0.115$ in a domain of length $20\pi/3$. At $t = 1500$, we add $\alpha e^{-4(v-2)^2}\cos(0.3x)$ to f, with $\alpha = 10^{-3}$ or 10^{-4}. Panel (a) plots $|\Phi_2|$ (solid), the running averages, $(t-1500)^{-1}\int_{1500}^{t}|\Phi_1|\,dt$ (dashed), and $|\Phi_1|$ for $\alpha = 10^{-4}$ (grey dots). Also shown is a simulation with $\alpha = 10^{-6}$ (dot-dashed). The stars indicate the times of the snapshots of (b)–(e).

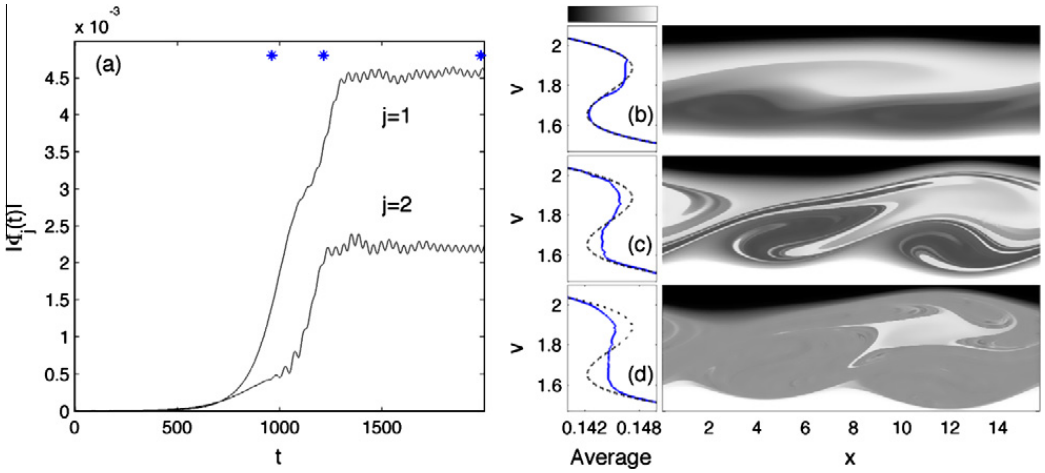

Fig. 10. Simulation with $a = 0.125$ in a domain of length 5π, initiated by adding the forcing, $10^{-3}te^{-10t^2}$, to the first two Fourier modes. Panel (a) shows $|\Phi_j|$ with $j = 1$ and 2. The stars indicate the times of the snapshots shown in (b)–(d).

Note that the perturbations of the BGK states in Fig. 9 are relatively strong: the mean amplitude of the fundamental mode is actually larger than that of the first overtone at the end of the computation for $\alpha = 10^{-3}$. Moreover, the dynamics is clearly quite different from that triggering the merger in Fig. 1. Thus, whether there is a genuine secondary instability or if the BGK state is simply strongly perturbed, mergers do not occur sufficiently close to the stability boundary. The BGK states certainly become more complicated as a result of the excitation of subharmonics: multiple frequencies are generated in the time series of the amplitude of the potential, satellite structures or quasi-particles form within the primary cat's-eyes [25], and there is a visible expansion of the regions over which the distribution is twisted-up. However, those state are long-lived.

A more curious example is shown in Fig. 10, with $a = 0.125$ and $L = 5\pi$. In this case, the lowest two modes are both unstable and their growth rates are comparable (see Fig. 2). Consequently, both modes grow and twist up the distribution into two separate cat's eye patterns surrounding the wave-particle resonances associated with each mode (which lie close to the two extrema of the equilibrium profile associated with the bump). The two patterns coexist for a time, but move at different speeds and perturb one another; eventually, the vortical structures within the cat's eyes interact more strongly, merging into a single structure. The double-mode character of the instability persists, however, with the distribution showing a mixed region with an embedded quasi-particle, bordered at lower velocity by a mode-two-like wave, and at higher speeds by a mode-one-like wave (this two-frequency state is quite different from those reported in [8], which are generated by the symmetrization of the initial bump-on-tail equilibrium distribution).

4. Discussion

The purpose of this article is to demonstrate that instabilities in the Vlasov–Poisson system display a rather richer, pattern-forming dynamics than is often discussed in the literature. We specifically focussed on the bump-on-tail instability, and showed that the BGK states which appear due to nonlinear saturation display complicated time-dependent dynamics near onset. Unlike what is often claimed in the literature, these BGK states need not suffer secondary, subharmonic instabilities that lead to coarsening of the wavelength; states with more than one wavelength in the spatial domain can persist indefinitely. As concluded previously for BGK modes of arbitrarily small amplitude, the secondary stability is closely related to the instabilities of the spatially homogeneous equilibrium that spawned the BGK states. Moreover, when secondary instabilities are present, they need not trigger wave mergers and coarsening, but precipitate complicated time-dependent states. In these regards, the Vlasov–Poisson system appears to have similarities with other pattern-forming systems.

It is unclear why previous explorations have not uncovered the dynamics found here. One possibility is that computations have never been run in the relevant range of parameter space: the dynamics is sensitive to distance from stability boundary as well as numerical resolution. Indeed, as illustrated by our first example, without careful selection of the initial state, the subharmonic instabilities can be sufficiently strong to overwhelm the dynamics we have described, and thereby trigger wave coarsening.

Although the study has been based on well-resolved numerical experiments, it is important to note that there are drawbacks with this kind of approach: subharmonic instability may take a long time to develop, and it is consequently difficult to say whether a computation has run sufficiently long to observe the true asymptotic states. Moreover, numerical inaccuracies and artifacts can cloud the true dynamics, especially for the Vlasov–Poisson system in which the main dynamical variable is inexorably wound up into increasingly fine filamentary structures. Overall, a numerical approach is always less conclusive than a rigorous stability analysis.

In addition, the BGK states that we have explored are not proper BGK modes: although nonlinearity saturates the linear instability relatively quickly, the cat's-eye patterns that form are continually winding up and agitated by aperiodic trapping oscillations. It is unclear whether these states ever converge fully to a true, steady BGK mode. Importantly, this means that there may be important differences between the current study and stability analyses of steady BGK equilibria [11,24,14,15].

Acknowledgements

For many years Phil Morrison has championed mathematical aspects of theoretical plasma physics and has interested many people from outside the plasma field in the outstanding issues. I thank Phil for introducing me to the Vlasov–Poisson problem and for many related discussions. I hope this contribution reawakens some interest in the nonlinear dynamics of Vlasov instabilities and prompts further work, mirroring Phil's many efforts along such lines.

References

[1] Armstrong TP, Montgomery D. Asymptotic state of the two-stream instability. J Plasma Phys 1967;1:425–33.
[2] Armstrong TP, Montgomery D. Numerical study of weakly unstable electron plasma oscillations. Phys Fluids 1969;12:2094–8.
[3] Balmforth NJ, Llewellyn Smith S, Young WR. Disturbing vortices. J Fluid Mech 2001;426:95–133.
[4] Balmforth NJ, Morrison PJ, Thiffeault J-L. Pattern formation in systems with continuous spectra and the single-wave model. Submitted to Rev Mod Phys; 2011.
[5] Bernstein IB, Greene JM, Kruskal MD. Exact nonlinear plasma oscillations. Phys Rev 1958;108:546–50.
[6] Cheng CZ, Knorr G. The integration of the Vlasov equation in configuration space. J Comput Phys 1976;22:330–51.
[7] Danielson JR, Anderegg F, Driscoll CF. Measurement of Landau damping and the evolution to a BGK equilibrium. Phys Rev Lett 2004;92:245003.
[8] Demeio L, Zweifel PF. Numerical simulations of perturbed Vlasov equilibria. Phys Fluids B 1990;2:1252–5.
[9] Dupree TH. Theory of phase-space density holes. Phys Fluids 1982;25:277–89.
[10] Ghizzo A, Izrar B, Bertrand P, Fijalkow E, Feix MR. Stability of Bernstein–Greene–Kruskal equilibria: numerical experiments over a long time. Phys Fluids 1988;31:72–82.
[11] Goldman MV. Theory of stability of large periodic plasma waves. Phys Fluids 1970;13:1281–9.
[12] Guo Y, Strauss WA. Instability of BGK equilibria. Commun Pure Appl Math 1995;63:861–984.
[13] Heath RE, Gamba IM, Morrison PJ, Michler C. A discontinuous Galerkin methods for the Vlasov–Poisson system. J Comp Phys. Submitted.
[14] Lin Z. Instability of periodic BGK waves. Math Res Lett 2001;8:1–14.
[15] Lin Z. Nonlinear instability of periodic BGK waves for the Vlasov–Poisson system. Commun Pure Appl Math 2005;58:505–28.
[16] Manfredi G. Long-time behaviour of nonlinear Landau damping. Phys Rev Lett 1997;79:2815–9.
[17] Manfredi G, Bertrand P. Stability of Bernstein–Greene–Kruskal modes. Phys Plasmas 2000;7:2425–31.
[18] Manneville P. Dissipative structures and weak turbulence. Academic Press; 1990. ISBN: 0124692605.
[19] Minardi E. Statistical thermodynamics of collisionless plasma. II. Stability theory of inhomogeneous systems. Plasma Phys 1972;14:443–8.
[20] Morrison PJ, Pfirsch D. Dielectric energy versus plasma energy, and action-angle variables for the Vlasov equation. Phys Fluids 1992;4B:3038–57.
[21] O'Neil TM. Collisionless damping of nonlinear plasma oscillations. Phys Fluids 1965;8:2255–62.
[22] O'Neil TM, Winfrey JH, Malmberg JH. Nonlinear interaction of a small cold beam and a plasma. Phys Fluids 1971;14:1204–12.
[23] Santini F. Electrostatic marginal stability of a one-dimensional inhomogeneous finite plasma. Plasma Phys 1970;12:165–73.
[24] Schwarzmeier JL, Lewis HR, Abraham-Schrauner B, Symon KR. Stability of Bernstein–Greene–Kruskal equilibria. Phys Fluids 1979;22:1747–60.
[25] Tennyson JL, Meiss JD, Morrison PJ. Self-consistent chaos in the beam-plasma instability. Physica D 1994;71:1–17.